Continuum mechanical modeling of axonal growth

Julián Andrés García-Grajales[a], Antoine Jérusalem[b], Alain Goriely[a]

[a] *Mathematical Institute, University of Oxford, Oxford, UK*
[b] *Department of Engineering Science, University of Oxford, Oxford, UK*

Abstract

Axonal growth is a complex phenomenon in which many intra- and extra-cellular signals collaborate simultaneously. Two different compartments can be identified in the growing axon: the growth cone, the leading tip that guides and steers the axon, and the axonal shaft, connecting the soma to the growth cone. The complex relations between both compartments and how their interaction leads the axon to its final synaptic target remain a topic of intense scrutiny. Here, we present a continuum and computational model for the development of the axonal shaft. Two different regions are considered: the axoplasm, filled with microtubules, and the surrounding cortical membrane, consisting mainly of F-actin, Myosin II motor proteins and the membrane. Based on the theory of morphoelasticity, the deformation gradient is decomposed into anelastic and viscoelastic parts. The former corresponds to either a growth tensor for the axoplasm, or a composition of growth and contractile tensors for the cortical membrane. The biophysical evolution for the anelastic parts is obtained at the constitutive level, in which the polymerization and depolymerization of microtubules and F-actin drive the growth, while the contractility is due to the pulling exerted by the Myosin II on the F-actin and depends on the stress. The coupling between cytoskeletal dynamics and mechanics is naturally derived from the equilibrium equations. The framework is exploited in two representative scenarios in which an external force is applied to the axonal shaft either along the axis or off the axis. In the first case three states are found: growth, collapse and stall. In the second case, axonal turning is observed. This framework is suitable to investigate the complex relationship between the local mechanical state, the cytoskeletal polymerization/depolymerization rates, and the contractility of the cortical membrane in axonal guidance.

Keywords: axonal guidance, axonal turning, continuum modeling, axonal elongation

Las neuronas son células de formas delicadas y elegantes, las misteriosas mariposas del alma, cuyo batir de alas quién sabe si esclarecerá algún día el secreto de la vida mental. Santiago Ramón y Cajal

1. Introduction

The pioneering work of Santiago Ramón y Cajal taught us that cognitive functions are carried out in the brain by neurons through synaptic connections (Cajal, 1909; DeFelipe and Jones, 1988; Pasik and Pasik, 1999). Neurons are electrical excitable cells that are morphologically divided into two different compartments: *the cell body* or *soma*, where the cell nucleus and other organelles are situated; and *the neurites*, which are thin tube-like processes extending from the soma and aimed at establishing synaptic connections with other processes of other neurons to create the neuronal network. The neurites can be classified into dendrites and axons: The electrical signal travels from the synapses to the soma for the former, and the signal is transmitted away from the soma to the synapses for the latter.

Neuronal growth is the key process necessary to establish the neuronal network during neurogenesis. Besides its vital role, neuronal growth also fulfills crucial functions in human brain plasticity (Pascual-Leone et al., 2005) and neuronal regeneration (Silver and Miller, 2004; Case and Tessier-Lavigne, 2005; Bradke et al.,

2012). In the early stages of neuronal development, multiple neurites sprout from the soma up to several micrometers, led by highly dynamical hand-shape terminations called *growth cones* (GCs). Eventually, one neurite specializes into the axon, while all the other neurites become dendrites (Goslin and Banker, 1989; Esch et al., 1999; Lewis et al., 2013). Once an axon is fully established, it can grow long distances navigating through a pool of chemo-mechanical cues and obstacles to find its final location (Goldberg, 2003; Debanne et al., 2011; Lewis et al., 2013).

Physical forces are one of the main actors throughout all scales in brain development, from molecular assembly of the neuron organelles to the final construction of the whole organ (Prevost et al., 2011; Goriely et al., 2015a,b; de Rooij and Kuhl., 2016). At the cell level, neuronal development is a complex problem that involves many intra- and extra-cellular interactions, e.g., forces, chemical gradients, substrate stiffness. During axonal growth, the growth cone is highly motile, while the axonal shaft (AS) connects it to the soma (Mitchinson and Kirschner, 1988), see Fig. 1-a. Forces in both domains, and particularly at the interface between them, are critical for proper axonal development (Athamneh and Suter, 2015). For example, the growth cone pulls on the axonal shaft by creating tension on it (Lamoureux et al., 1989; Zheng et al., 1991; Heidemann and Buxbaum, 1994; Lamoureux et al., 1998), suggesting that growth cone pulling is the driving force for axonal elongation. Conversely, other works suggest that there is contribution of the axonal shaft which pushes and propels the growth cone (Marsh and Letourneau, 1984; Lafont et al., 1993; Dogterom and Yurke, 1997; Dogterom et al., 2005). As a consequence, axonal growth can be considered as arising from the coupling between the growth cone and the axonal shaft, as an orchestrated phenomenon in which each part of the axon is playing a crucial mechanical role (Franze and Guck, 2010; Athamneh and Suter, 2015).

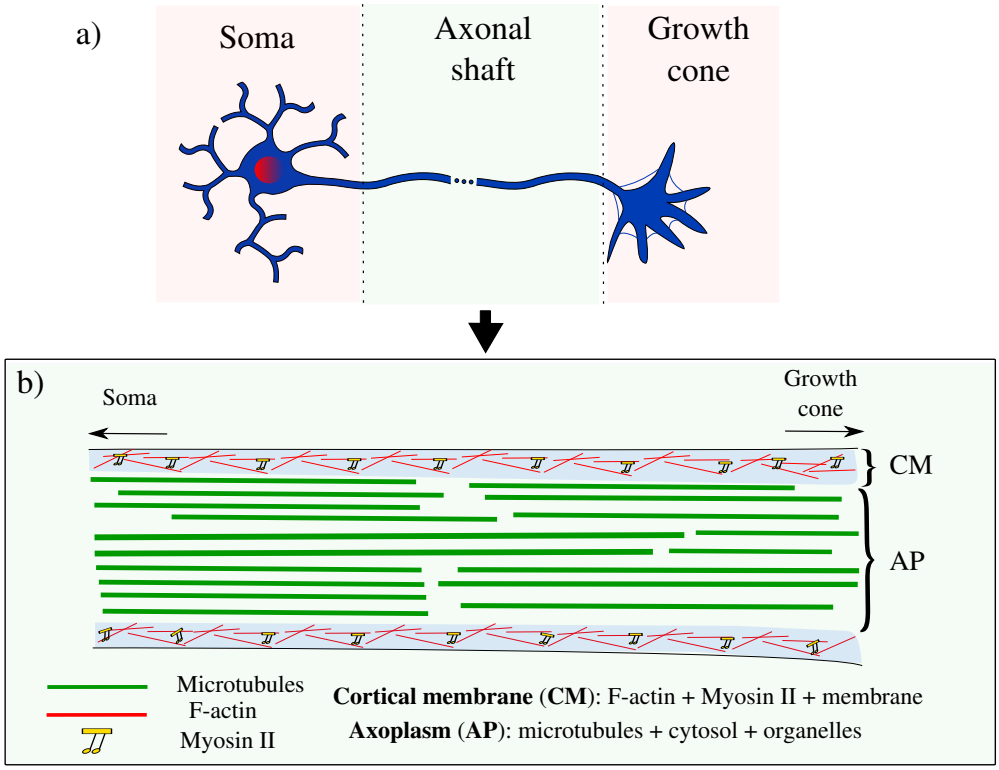

Figure 1: Schematic representation of the different compartments during neuronal development. a) The axon is split into an axonal shaft (AS) and a growth cone (GC). The axonal shaft is a tube-like that connects the growth cone to the soma, whereas the growth cone is the highly motile and dynamic tip of the axon, that processes all external and internal chemo-mechanical signals. b) axonal shaft zoom-in. Two different domains are considered here: the axoplasm, which is the inner core of the axonal shaft; and the cortical membrane, which is the surrounding complex that wraps the axoplasm.

The main structural scaffold of the neuron, *the cytoskeleton* (Fletcher and Mullins, 2010), is an evolving

dynamic polymeric structure that is actively involved in axonal outgrowth (Stiess and Bradke, 2009). The cytoskeleton is composed of three main types of filamentous polymers: F-actin, microtubules and neurofilaments. Neurofilaments are passive and apolar polymers. Despite being the most abundant cytoskeletal filaments in the axon, they are not believed to contribute to axonal growth (Foisner, 2002; Fletcher and Mullins, 2010; Franze and Guck, 2010). The two other polymers, F-actin and microtubules, are highly dynamic and polarized. The former polymerizes at one end (barbed-end) by addition of G-actin and depolymerizes at the other end (pointed-end) by removal of monomers, while the latter polymerizes at one end (plus-end) by addition of tubulin dimers and depolymerizes at the other end (minus-end) by removal of monomers (Coles and Bradke, 2015). While microtubules are the stiffest cytoskeleton components (Conde and Cáceres, 2009) and F-actin are less rigid on their own, the latter are able to build organized stiff structures thanks to the presence of high concentrations of crosslinkers (Fletcher and Mullins, 2010). Their complex interactions as well as their relations with the surrounding structures and associated motor proteins (e.g., Dynein or Kinesin for microtubules or Myosin II for F-actin) are crucial for proper axonal development (Stiess and Bradke, 2009). They also are heterogeneously distributed along the axon domain (Mitchinson and Kirschner, 1988; Edward, 2009). In the growth cone, microtubules are less expressed than the F-actin. However, their interactions condition the growth cone navigation (e.g., turning and steering) (Geraldo and Gordon-Weeks, 2009), or the axonal elongation by means of promoting the polymerization of the microtubule array linked to the axon growth (Dent et al., 2011). Furthermore, F-actin filaments also participate in filopodia protrusion and thus growth cone navigation (Dent et al., 2011; Gomez and Letourneau, 2014; Goodhill et al., 2015). In the axonal shaft, the distribution of microtubules and F-actin is different, see Fig. 1-b. Despite the fact that a mature axon cytoskeletal structure is known to have a periodic ring distribution (Xu et al., 2013), when considering the growth of the axonal shaft, two regions can be identified with different filaments arrays: the inner core of the axonal shaft, *the axoplasm*, and the surrounding complex, *the cortical membrane*. The axoplasm is filled with para-axially aligned bundles of microtubules, the cytosol and other organelles. Microtubules are crosslinked by microtubule-associated-proteins, *tau proteins*, that provide mechanical integrity to the lattice (Edward, 2009; Ahmadzadeh et al., 2014). The dynamic tips of the microtubules (plus-end) are pointing towards the distal tip of the axon (Baas et al., 1988). On the other hand, the cortical membrane groups the membrane, Myosin II and F-actin. The latter are mainly surrounding the axoplasm and with the presence of Myosin II proteins participate to the contractility of the axonal shaft (Jülicher et al., 2007; Coles and Bradke, 2015).

Computational and mathematical modeling are valuable tools that can help to overcome the technical experimental limitations when studying complex problems such as neuronal development. Numerous authors have explored the mathematical modeling of neurite outgrowth with a variety of approaches (see reviews of Graham et al. (2006) and van Ooyen (2011)). Different mathematical techniques are used to model the stages during the neurite outgrowth: initiation, elongation, axon pathfinding, and branching. These mathematical approaches generally consider one-dimensional cases for the neurite development, evolving in two-dimensional environments (Graham et al., 2006). Elongation and axonal pathfinding stages have been widely explored. One of the most complete axonal guidance model was presented by M. Aeschlimann and coworkers in 2000 (Aeschlimann, 2000; Aeschlimann and Tettoni, 2001). The model is a one-dimensional representation of a neurite that navigates in a two-dimensional extra-cellular substrate, led by the growth cone and the filopodia dynamics. Moreover, several tubulin-driven models have been proposed for the axonal elongation under the assumption that neurite growth is led by microtubule dynamics (van Veen and van Pelt, 1994; Miller and Samuels, 1997; McLean et al., 2004; Graham et al., 2006; van Ooyen et al., 2001; Graham and van Ooyen, 2001; Poulain and Sobel, 2010; García et al., 2012; Diehl et al., 2014, 2016). A robust software aimed at modeling the growth and development of the neurons was proposed by Zubler and Douglas (2009). This open-source framework, called CX3D, provides a three-dimensional scenario to explore, among other capabilities, the extension of neurites as well as the contact between the neurites and the somas when the neurites are growing, by means of the compartmental modeling approach. Recently, CX3D has been extended to explore the growth cone guidance in function of the extra-cellular chemical guidance cues (Roccasalvo et al., 2015). Continuum finite deformation approaches are much scarcer when modeling neuronal growth (Goriely et al., 2015a). Recently, Kuhl and coworkers have explored the axonal elongation (fiber growth with a constant axonal growth rate) as the cause of the folding of our brain (Budday et al., 2014;

Holland et al., 2015). Such continuum approaches rely on the decomposition of the deformation gradient into an elastic and growth parts, originally introduced in the context of biological tissues by Rodriguez et al. (1994). Despite tremendous efforts in modeling neurite outgrowth, a fully unified two- and three-dimensional continuum framework that accounts for the various biological, chemical, and mechanical interactions is still lacking. As such, the development a full three-dimensional framework appears as a valuable tool to explore the differences between axonal growth and development (including axonal guidance) when modelled in a one-dimensional fashion and when modelled in a three-dimentsional fashion. If the following general framework is thus developed in three dimensions, the proposed study focuses first on two dimensions, which is the lowest dimension allowing for a cross-sectional differentiation of the mechanical properties. This, in turn, allows for a characterization of the turning ability of a neuron. In the long run, the aim is to use such a model in a 3D environment, closer to a brain setting.

Based on the theoretical previous study carried out by Recho et al. (2016) and on the theory of the active gel proposed by Jülicher et al. (2007), we present a fully three-dimensional continuum mechanical model for axonal shaft development. Here, we develop a framework based on the decomposition of the deformation gradient into elastic and anelastic parts. For the former, a viscoelastic constitutive model is used for the whole axonal shaft, while for the latter, the anelastic part corresponds to the growth for the axoplasm and to a composition of growth and contractility for the cortical membrane. The coupling between cytoskeletal dynamics and mechanics is naturally derived from the equilibrium equations. This framework is implemented in our dedicated finite elements and meshless methods program *OXFEMM* (**O**xford **F**inite **E**lements and **M**eshless **M**ethods). Here, we illustrate this approach on a simpler two-dimensional version of the problem to study the static, collapse and growth states of the axon, as well as axonal turning. Axonal growth velocity appears as a balance between the contributions of the axoplasm, the cortical membrane, the geometrical link between them, and the external hypothetical force applied by the growth cone. Moreover, we show that the coupling between the cytoskeletal dynamics (polymerization/depolymerization rates at constant concentration along the entire domain) and mechanics, as well as the contractility of the cortical membrane, play a crucial role in axonal steering. This finding suggests that the growth cone can act in axonal guidance as a trigger growth rate modulator at its interface with the axonal shaft.

2. Continuum framework for axonal development

2.1. Kinematics

A material point initially at the position $\mathbf{X}$ in the reference configuration of the domain $\boldsymbol{\Omega}_0$ is related to its final position $\mathbf{x}$ in the current configuration $\boldsymbol{\Omega}_t$ through the displacement field:

$$\mathbf{u}(\mathbf{X}) = \mathbf{x} - \mathbf{X}, \qquad \mathbf{x} = \boldsymbol{\chi}(\mathbf{X}), \tag{1}$$

where $\boldsymbol{\chi}$ is an invertible mapping describing all deformation processes, see Figure 2. To model the final deformation state, the key kinematic quantity in the context of finite deformation is *the deformation gradient*, defined as $\mathbf{F} = \nabla\boldsymbol{\chi}(\mathbf{X})$.

In general, the response of materials to mechanical constraints can be classified into two different sets of deformation: an elastic response and an anelastic part, e.g., plastic flow, growth (Rodriguez et al., 1994). The driving anelastic processes of axonal elongation considered here are the growth of the axoplasm, and the growth and contractility of the cortical membrane. Such processes are modeled by the multiplicative decomposition of $\mathbf{F}$ as follows:

$$\mathbf{F} = \mathbf{F}_e \cdot \mathbf{F}_a. \tag{2}$$

A useful way to picture this decomposition is to consider the two steps: First, the material evolves from its natural reference state $\boldsymbol{\Omega}_0$ to the virtual stress-free $\boldsymbol{\Omega}_v$ configuration, due to a pure anelastic map $\mathbf{F}_a$ (compatible or not). Second, the material deforms from $\boldsymbol{\Omega}_v$ to $\boldsymbol{\Omega}_t$ due to the application of the elastic mapping $\mathbf{F}_e$, see Figure 2. This latter step ensures the compatibility of the whole deformation and does not add mass to the system (Ben Amar and Goriely, 2005). There are many biological applications in the literature using this approach. For instance, when $\mathbf{F}_a$ is considered as growth, this decomposition has been

used for different applications, ranging from morphogenesis at cellular and sub-cellular scales to plant and animal physiology growth (Goriely et al., 2010; Ambrosi et al., 2011; Moulton and Goriely, 2011; Kuhl, 2014; Eskandari and Kuhl, 2015; Budday et al., 2015).

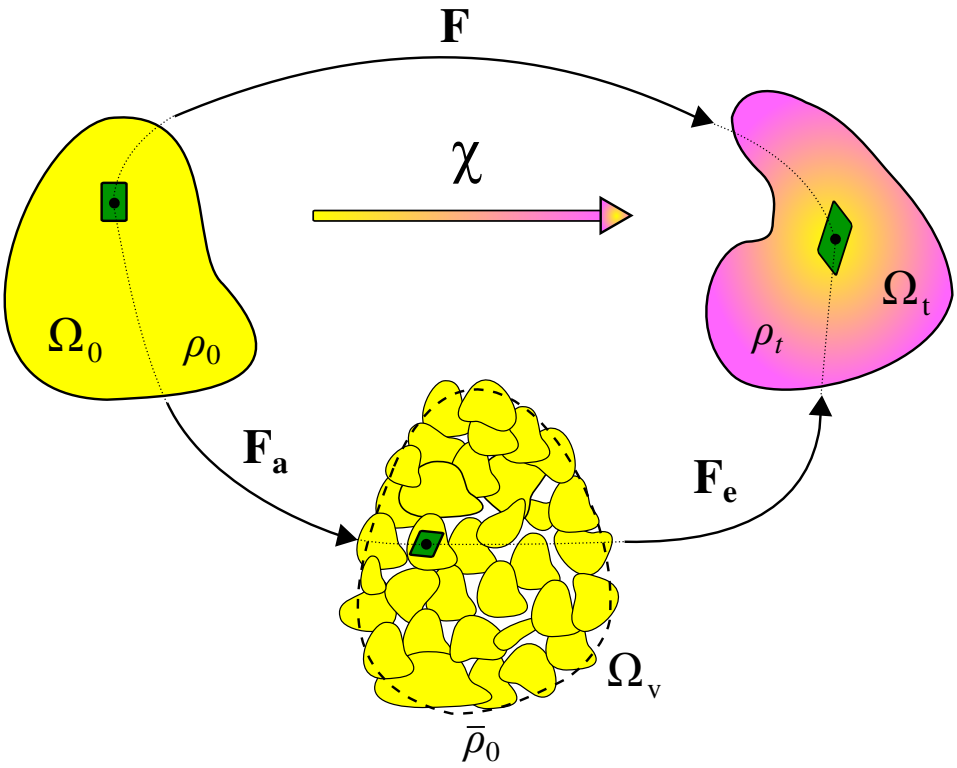

Figure 2: Deformation process.

2.2. Balance laws

The balance of angular momentum is automatically satisfied constitutively by assuming that the Cauchy stress tensor is symmetric, while the balance of linear momentum in the reference configuration $\mathbf{\Omega}_0$ is given by:

$$\mathrm{Div}\,\mathbf{P} + \rho_0 \mathbf{b} = \rho_0 \ddot{\mathbf{u}}, \tag{3}$$

where $\mathbf{P}$ is the first Piola-Kirchhoff stress tensor, $\mathbf{b}$ are the body forces, $\ddot{\mathbf{u}}$ is the point acceleration, and ρ_0 is the natural density.

The density evolves during the deformation from the reference configuration density ρ_0, to its counterpart at the current time t, $\rho(\mathbf{x}, t)$, passing by the density in the intermediary configuration $\bar{\rho}_0$, see Figure 2. It follows from Equation (2) that

$$J = J_e J_a, \tag{4}$$

where $J = \det \mathbf{F} > 0$, $J_e = \det \mathbf{F}_e > 0$ and $J_a = \det \mathbf{F}_a > 0$. The mass balance between the intermediary and the current configurations, see Figure 2, leads to the following relation:

$$J_e = \frac{\bar{\rho}_0}{\rho_t} \tag{5}$$

where the dynamic evolution of ρ_t, can be obtained by differentiating Equation (5) as follows:

$$\dot{\rho}_t = \rho_t \left(\bar{\rho}_0^{-1} \dot{\bar{\rho}}_0 - J_e^{-1} \dot{J}_e \right) \tag{6}$$

By differentiating Equation (4) and noting that $\dot{J} = J\mathrm{div}\,\mathbf{v}$, where $\mathbf{v}$ is the velocity, the rate of change in volume during the elastic deformation $\dot{J}_e$ is defined by:

$$\dot{J}_e = J_e \left(\mathrm{div}\,\mathbf{v} - J_a^{-1}\dot{J}_a \right), \tag{7}$$

Finally, gathering Equations (6) and (7), the final mass balance law reads:

$$\dot{\rho}_t + \rho_t \mathrm{div}\,\mathbf{v} = \underbrace{\rho_t \left(\bar{\rho}_0^{-1}\dot{\bar{\rho}}_0 + J_a^{-1}\dot{J}_a \right)}_{s}, \tag{8}$$

where s is the source term for the addition of mass. The form of s can be determined by a suitable definition of the evolution of $\bar{\rho}_0$ and/or J_a. In our particular problem, we consider that all material addition is coming from the anelastic component itself and not from any other source, while the elastic component ensures material compatibility, so that we have $\dot{\bar{\rho}}_0 = 0$. The source term is thus reduced to:

$$s = \rho_t J_a^{-1}\dot{J}_a. \tag{9}$$

2.3. A continuum model for axonal growth

Following the general description of Recho et al. (2016), we model a growing axon as a continuum structure with two different compartments: the axoplasm and the cortical membrane. Note that the growth cone is not explicitly represented as a compartment and its effect is modeled through the boundary tractions at the distal end of the axon. In the present work each compartment is itself a two- or three-dimensional structure and is modeled as an anelastic structure through the usual multiplicative decomposition of the deformation gradient given by Equation (2). The axoplasm is assumed to be morphoelastic (Goriely and Moulton, 2010), i.e., we use the anelastic part of the deformation gradient $\mathbf{F}_a$ to model growth along the axis. The cortical membrane is assumed to be both growing and contracting. To model this effect, we further decompose the anelastic part of the deformation gradient $\mathbf{F}_a$ into contractile and growing parts. We also assume that the stresses relax in time through visco-elastic relaxation following a first-order generalized Maxwell model. The detailed models for each component is given next.

2.3.1. Axoplasm model

It is assumed here, that the overall growth of the axon is directly linked to the polymerization and depolymerization of its cytoskeletal filaments. We can directly apply the decomposition presented in Equation (2), schematically shown in Figure 2, by defining:

$$\mathbf{F}_a := \mathbf{F}_g, \tag{10}$$

where $\mathbf{F}_g$ is the growth tensor that provides the evolution of the *fiber growth*, in which growth occurs in one preferential direction $\mathbf{n}_0$ (Goriely et al., 2010; Kuhl, 2014) as follows:

$$\mathbf{F}_g = \mathbf{I} + [\gamma_{ap} - 1]\mathbf{n}_0 \otimes \mathbf{n}_0, \tag{11}$$

where γ_{ap} is the growth multiplier that governs the growth in the $\mathbf{n}_0$ direction (the axisymmetric axis of the axon), thus implying that there is no growth in the cross-fiber direction. Under such assumptions, an increment of γ_{ap} represents the corresponding change in volume due to growth J_g, $\gamma_{ap} = J_g$. Assuming that the mass addition in the axoplasm is due to the dynamics of the microtubules, the source term s in Equation (9) takes the following form:

$$s = \rho_t^{ap}\gamma_{ap}^{-1}\dot{\gamma}_{ap} = k_p^{ap} - k_d^{ap}\rho_t^{ap}, \tag{12}$$

where the right hand side corresponds to a first-order kinetic expression with the rate constants k_p^{ap} and k_d^{ap}, the polymerization and depolymerization rates of the microtubules, respectively. Here, ρ_t^{ap} is the density

of microtubules in the axoplasm in the current configuration (mass of microtubules/volume of axoplasm). The concentration of tubulin dimers available in the axoplasm is assumed constant and homogeneous, i.e., diffusion or active transport of tubulin dimers are not considered in this model. Finally, with Equation (5), the growth evolution of the axoplasm reads:

$$\dot{\gamma}_{ap} = \frac{J}{\rho_0^{ap}} k_p^{ap} - k_d^{ap} \gamma_{ap}, \tag{13}$$

where the relation between mechanics ($\mathbf{F}$) and growth (γ_{ap}) is obtained through the change in volume J.

2.3.2. Cortical membrane model

Two effects are considered in our model for the cortical membrane: contractility of the cortical membrane complex and its growth. Mathematically, it implies that the anelastic part in Equation (2) is split further into two steps (see Figure 3):

$$\mathbf{F}_a := \mathbf{F}_c \cdot \mathbf{F}_g \tag{14}$$

leading to a decomposition of $\mathbf{F}$ into three steps:

$$\mathbf{F} = \mathbf{F}_e \cdot \mathbf{F}_c \cdot \mathbf{F}_g \tag{15}$$

where the deformation process can be understood as follows: 1) the material evolves from its natural initial state $\mathbf{\Omega}_0$ to a virtual stress-free $\mathbf{\Omega}_{v1}$ configuration due to pure growth $\mathbf{F}_g$; 2) the material experiences an active contraction from $\mathbf{\Omega}_{v1}$ to $\mathbf{\Omega}_{v2}$, due to the work done by the Myosin motor proteins on the F-actin network $\mathbf{F}_c$; and 3) the material deforms from $\mathbf{\Omega}_{v2}$ to $\mathbf{\Omega}_t$ according to a constitutive relation due to the application of $\mathbf{F}_e$, see Figure 3. The last jump from the virtual configuration to the current one guarantees that the total deformation is compatible and satisfies the boundary conditions (Ben Amar and Goriely, 2005; Himpel et al., 2005). This last step does not add mass to the system

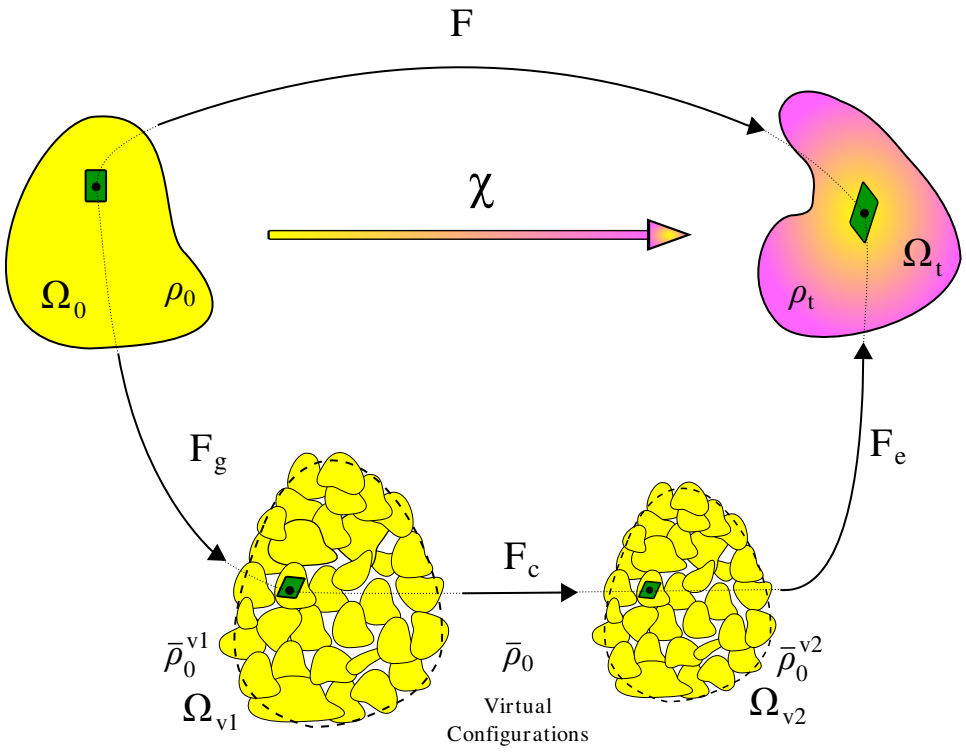

Figure 3: Cortical membrane deformation process.

For the cortical membrane, we follow the same steps and introduce a fiber growth tensor $\mathbf{F}_g$

$$\mathbf{F}_g = \mathbf{I} + [\gamma_{cm} - 1]\mathbf{n}_0 \otimes \mathbf{n}_0 \tag{16}$$

where γ_{cm} is the growth multiplier that governs the growth in the $\mathbf{n}_0$ direction corresponding with the axonal axis. We have again, $\gamma_{cm} = J_g$. The derivation of the balance of mass presented in Section 2.2, can be used for the cortical membrane as long as the contractile part is considered incompressible, i.e., there is no change in volume due to contractility ($J_c = \det \mathbf{F}_c = 1$). Assuming that mass addition in the cortical membrane is due to the dynamics of the F-actin, the source term s in Equation (9) takes the following form:

$$\rho_t^{cm} \gamma_{cm}^{-1} \dot{\gamma}_{cm} = k_p^{cm} - k_d^{cm} \rho_t^{cm}, \tag{17}$$

where the right-hand-side corresponds to a first-order kinetic equation with the rate constants k_p^{cm} and k_d^{cm}, the polymerization and depolymerization rates of the F-actin, respectively. Here, ρ_t^{cm} is the density of F-actin in the cortical membrane in the current configuration. Finally, with Equation (5), the growth evolution of the cortical membrane reads:

$$\dot{\gamma}_{cm} = \frac{J}{\rho_0^{cm}} k_p^{cm} - k_d^{cm} \gamma_{cm}. \tag{18}$$

In order to model the evolution of the contractile tensor $\mathbf{F}_c$ (initialised as the identity tensor $\mathbf{I}$ at $t = 0$), we use the following physically-motivated relation:

$$\dot{\mathbf{F}}_c = -c_{cm}\ \mathbf{n}_0 \otimes \mathbf{n}_0, \text{ with } \det \mathbf{F}_c = 1, \text{ and } \mathbf{F}_c(t = 0) = \mathbf{I}, \tag{19}$$

where c_{cm} is the contractility rate in the direction $\mathbf{n}_0$, along the axis of the axon. The evolution of c_{cm} is assumed to follow:

$$\begin{cases} c_{cm} = 0, & \text{if } \bar{\sigma} \leq 0 \text{ or } \bar{\sigma} > \sigma_0 \\ c_{cm} = c_{cm}^0 \left(1 - \dfrac{\bar{\sigma}}{\sigma_0}\right), & \text{otherwise} \end{cases} \tag{20}$$

where $\bar{\sigma} = \boldsymbol{\sigma} : \mathbf{n}_0 \otimes \mathbf{n}_0$ and $\boldsymbol{\sigma}$ is the Cauchy stress. Physically, Equation (20) represents the activity of the Myosin motor proteins pulling the F-actin and creating contractile stress, that is modeled here through the specification of an active strain. The contractility rate c_{cm} is zero when the projection of the stress in the relevant direction $\mathbf{n}_0$ is zero or is in compression, i.e., the Myosin does not create any contractility under compression or stress-free states, (Jülicher et al., 2007). If the region is in a state of tension below a threshold σ_0, the Myosin II motor proteins induce contractility at a rate that is decreasing as the tension increases. When the tension is larger than σ_0, Myosin motor proteins are deactivated and $c_{cm} = 0$.

2.3.3. Constitutive response: viscoelasticity

The anelastic parts of the deformation gradient are considered stress-free during the entire process—compatible or not—while $\mathbf{F}_e$ recovers the compatibility of the deformation (Rodriguez et al., 1994). Forces play a major role in the interactions between the different compartments of the axon when it is growing, e.g., growth cone on axonal shaft, axonal shaft on the growth cone, and other domains within the growth cone, (Lu et al., 2006; Betz et al., 2011; O'Toole et al., 2015; Recho et al., 2016). The overall mechanical behavior of the axon, i.e., how the stresses are connected with the strains, depends on the time scales at which these mechanical processes take place. Axons behave like solids at short time scales, while at long time scales they behave more in a fluid manner (Dennerll et al., 1989; Bernal et al., 2007; O'Toole et al., 2008; Javid et al., 2014; Ahmadzadeh et al., 2014). Other studies have shown that the mechanical response is heterogeneous along the entire axon, exhibiting solid-like response in the soma, stiffer viscous-like response in the neurites, with the axonal shaft less viscous than the growth cone (O'Toole et al., 2015; Grevesse et al., 2015).

In view of these evidences, and taking into account the time scale at which axonal growth takes place ($\sim 10\ \mu m/h$), we model here the axonal shaft as a viscoelastic material by means of a first-order generalized Maxwell model (Simo and Hughes, 1998), with $\mathbf{F}_e := \mathbf{F}_v$, see Figure 4. Conceptually, the axon is solid-like

at very short time scale, viscous-like at intermediate times in which both elastic and viscous contributions will produce a flow response (e.g, axonal outgrowth), and solid-like again over long time scales (e.g., growth over days or years). The final behavior observed depends crucially on the time constant associated with the elastic (E, the Young's modulus) and viscous (η, viscous coefficient) response in the Maxwell branch: $\tau = \eta/E$ (in the order of seconds for cells, see Betz et al. (2011); Jülicher et al. (2007)). The constitutive model used in this work is the one proposed by Simo and Hughes (1998) for finite viscoelasticity.

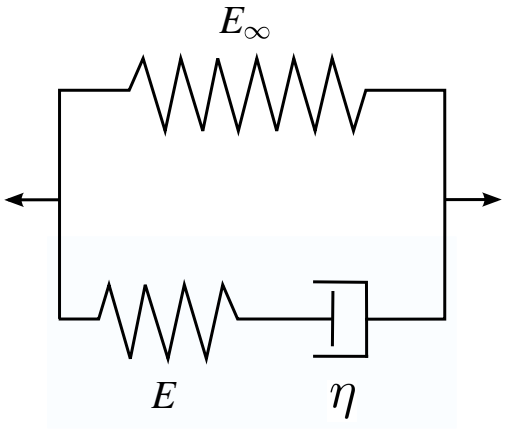

Figure 4: First-order generalized Maxwell model. This figure is a schematic representation of the viscoelastic model and is aimed at following the formulation proposed by Simo and Hughes (1998). See also Prevost et al. (2011) and de Rooij and Kuhl. (2016).

The deformation is decomposed into a volume-preserving deviatoric part and a volumetric part. The former is characterized by:

$$\bar{\mathbf{F}} = J_v^{\frac{1}{3}}\,\mathbf{F}_v, \tag{21}$$

where $J_v = \det \mathbf{F}_v > 1$ and $\det \bar{\mathbf{F}} = 1$. The corresponding right Cauchy-Green tensors are defined by:

$$\begin{cases} \mathbf{C} = \mathbf{F}_v^T \cdot \mathbf{F}_v, \\ \bar{\mathbf{C}} = \bar{\mathbf{F}}^T \cdot \bar{\mathbf{F}}. \end{cases} \tag{22}$$

The Kirchhoff stress $\boldsymbol{\tau}$ tensor is given by:

$$\boldsymbol{\tau} = J_v U^{o\prime}(J_v)\mathbf{I} + \int_{-\infty}^{t} g(t-s)\frac{d}{ds}\left(\text{dev}\left\{2\bar{\mathbf{F}}\cdot\frac{\partial \bar{W}^o}{\partial \bar{\mathbf{C}}}\cdot\bar{\mathbf{F}}^T\right\}\right)ds, \tag{23}$$

where $U^o(J_v)$ and $W^o(\bar{\mathbf{C}})$ are the volumetric and volume-preserving components of the stored-energy function,

$$W^o(\mathbf{C}) = U^o(J_v) + \bar{W}^o(\bar{\mathbf{C}}). \tag{24}$$

The function g is the relaxation function associated with the standard linear solid model and defined as:

$$g(t) = G_\infty + G\,\exp(-t/\tau), \tag{25}$$

where $G_\infty = E_\infty/E_0$ (with $E_0 = E_\infty + E$), and $G = E/E_0$, see Figure 4.

In this constitutive model, the internal variables can be interpreted as the inelastic strain in the dashpot (see Simo and Hughes (1998) for details).

3. Computational approach: incremental formulation

Next, we present the algorithmic implementation of the finite growth framework exposed in the previous section in the context of the finite-elements method. The implementation is carried out in our in-house program *OXFEMM*. In view of the scale of the problem, the use of the explicit scheme would lead to impracticable time steps Δt. A static implicit scheme is thus used here—although its dynamic version is also available in *OXFEMM*. At each time step, *OXFEMM* solves Equation (3) in a total Lagrangian formulation by means of the finite-element technique. It thus requires from the constitutive model, the first Piola-Kirchhoff stress tensor $\mathbf{P}$ and the tangent moduli

$$\mathbb{C} = \frac{d\mathbf{P}}{d\mathbf{F}}. \tag{26}$$

The time discretization is aimed at capturing all the phenomena involved in our particular problem, e.g., polymerization, contractility, viscoelasticity. In order to advance in time, i.e., $t_{n+1} = t_n + \Delta t_n$, the previous state n of the following variables are known at each integration point: $\mathbf{F}^{n+1}$, $\mathbf{F}^n$, $\mathbf{F}_c^n$, $\mathbf{P}^n$, γ^n, c_{cm}^n, as well as the corresponding internal variables of the vicoelastic model, $\tilde{\mathbf{S}}_n^o$ and $\mathbf{H}_n$ (see Section 3.3 and Simo and Hughes (1998)).

3.1. Time discretization of growth

The evolution of the growth tensors of the two different domains in the axonal shaft, i.e., the axoplasm and cortical membrane, is governed by the rate of growth in the corresponding direction $\mathbf{n}_0$ given by Equations (13) and (18). The implicit finite difference time discretization of those equations leads to:

$$\gamma_i^{n+1} = \frac{\gamma_i^n + \frac{J_{n+1} k_p^i \Delta t_n}{\rho_0^i}}{1 + k_d^i \Delta t_n}, \quad \forall i \in \{ap, cm\} \tag{27}$$

where the growth multiplier γ_i^{n+1} at the end of the time step Δt_n depends on the current J_{n+1}.

In the particular case where J is constant and γ is initially equal to one, The linear Equations (13) and (18) can be directly integrated. Initially, the growth rate evolves linearly, decreasing or increasing depending on J, and then converges exponentially to an asymptotic value $\gamma \to (J k_d^i)/(\rho_0^i k_p^i)$.

3.2. Time discretization of contractility

Equation (19) is also discretized as follows:

$$\mathbf{F}_c^{n+1} = \mathbf{F}_c^n + c_{cm}^{n+1}\ \mathbf{n}_0 \otimes \mathbf{n}_0, \text{ and } \det \mathbf{F}_c^{n+1} = 1, \tag{28}$$

where c_{cm}^{n+1} is defined by a direct explicit application of Equation (20),

$$\bar{\sigma}^{n+1} = \boldsymbol{\sigma}^n : \mathbf{n}_0 \otimes \mathbf{n}_0 \tag{29}$$

where $\boldsymbol{\sigma}^n$ is the Cauchy stress of the previous time step. In all simulations, the time convergence was systematically verified by decreasing systematically the time step. Similarly the mesh size was decreased in some simulations to check spatial convergence. In both cases, spatial or temporal convergence were not found to be an issue.

3.3. Stress compatibility

Once $\mathbf{F}_g^{n+1}$ and $\mathbf{F}_c^{n+1}$ are defined, see Sections 3.1 and 3.2, the anelastic part of the deformation $\mathbf{F}_a^{n+1}$ is known, the viscous component is then calculated as follows:

$$\mathbf{F}_v^{n+1} = \mathbf{F}^{n+1} \cdot (\mathbf{F}_a^{n+1})^{-1}. \tag{30}$$

where $\mathbf{F}^{n+1}$ is the deformation gradient at time t_{n+1} provided by the finite element framework to the constitutive model.

The viscous internal variables consist of two tensors: $\tilde{\mathbf{S}}_n^o$ and $\mathbf{H}_n$. At the end of the time increment, $\boldsymbol{\tau}_{n+1}$ is defined by:

$$\boldsymbol{\tau}_{n+1} = J_v^{n+1} U^{o\prime}(J_v^{n+1})\mathbf{I} + g(\Delta t_n)\bar{\boldsymbol{\tau}}_{n+1}^o + \bar{\boldsymbol{h}}_n, \tag{31}$$

where $g(\Delta t_n)$ is defined by Equation (25). The $\bar{\boldsymbol{\tau}}_{n+1}^o$ is defined by:

$$\bar{\boldsymbol{\tau}}_{n+1}^o = \mathrm{dev}\left[2\bar{\mathbf{F}}_{n+1} \cdot \frac{\partial \bar{W}^o(\bar{\mathbf{C}}_{n+1})}{\partial \bar{\mathbf{C}}} \cdot \bar{\mathbf{F}}_{n+1}^T\right], \tag{32}$$

and, $\bar{\boldsymbol{h}}_n$ is defined as:

$$\bar{\boldsymbol{h}}_{n+1} = G\mathrm{dev}\left[\bar{\mathbf{F}}_{n+1} \cdot \tilde{\mathbf{H}}_n \cdot \bar{\mathbf{F}}_{n+1}^T\right]. \tag{33}$$

where $\tilde{\mathbf{H}}_n$ is given by:

$$\tilde{\mathbf{H}}_n = \exp(-\Delta t_n/\tau)\mathbf{H}_n - \exp(-\Delta t_n/2\tau)\tilde{\mathbf{S}}_n^o. \tag{34}$$

The last step consists in updating the internal variables as follows:

$$\begin{aligned} \tilde{\mathbf{S}}_{n+1}^o &= \bar{\mathbf{F}}_{n+1}^{-1} \cdot \bar{\boldsymbol{\tau}}_{n+1}^o \cdot \bar{\mathbf{F}}_{n+1}^{-T}, \\ \mathbf{H}_{n+1} &= \tilde{\mathbf{H}}_n + \exp(-\Delta t_n/2\tau_1)\tilde{\mathbf{S}}_{n+1}^o. \end{aligned} \tag{35}$$

Note that $\mathbf{P}_{n+1}$ is easily obtained as follows:

$$\mathbf{P}_{n+1} = \boldsymbol{\tau}_{n+1} \cdot (\mathbf{F}_v^{n+1})^{-T}. \tag{36}$$

When solving implicitly, the tangent moduli $\mathbb{C}_{n+1}$ is also required and obtained from Equation (30) (in index notation and dropping the $n+1$ labels for clarity) as follows:

$$\mathbb{C}_{n+1} = \frac{\partial P_{ij}}{\partial F_{kl}} = \underbrace{\frac{\partial P_{ij}}{\partial (F_v)_{pq}}}_{\bar{\mathbb{C}}_{n+1}} \underbrace{\left((F_a^{-1})_{pm}\frac{\partial F_{mq}}{\partial F_{kl}} + \frac{\partial (F_a^{-1})_{pm}}{\partial F_{kl}}F_{mq}\right)}_{\frac{\partial (F_v)_{pq}}{\partial F_{kl}}}, \tag{37}$$

where the two different factors on the right-hand side, $\bar{\mathbb{C}}_{n+1}$ and $\frac{\partial (F_v)_{pq}}{\partial F_{kl}}$, can be interpreted as the contributions of the viscous part and of the decomposition itself to $\mathbb{C}$, respectively. Moreover, noting the relationship between the Kirchhoff stresses, $\mathbf{S} = \mathbf{F}^{-1} \cdot \mathbf{P}$ (dropping again $n+1$), the following relationship can obtained:

$$\tilde{\mathbb{C}} = \mathbf{I} \otimes \mathbf{S} + [\mathbf{F}_v \otimes \mathbf{I}]\bar{\mathbb{C}}[\mathbf{F}_v \otimes \mathbf{I}]^T, \tag{38}$$

where the product $\otimes$ between two second-order tensors $\mathbf{B}$ and $\mathbf{D}$ is defined as $(\mathbf{B}\otimes\mathbf{D})_{ijkl} = B_{ik}D_{jl}$ (Curnier, 1994), and the material tangent moduli

$$\bar{\mathbb{C}}_{n+1} = 2\frac{d\mathbf{S}_{n+1}}{d\mathbf{C}_{n+1}}, \tag{39}$$

can directly be obtained from Simo and Hughes (1998).

The last term in Equation (37) is difficult to evaluate. However, as growth is expected to be a slow process with respect to the time step, one can assume that $\frac{\partial \mathbf{F}_a^{-1}}{\partial \mathbf{F}} \sim \mathbf{0}$ without loss of convergence:

$$\frac{\partial \mathbf{P}}{\partial \mathbf{F}} = \tilde{\mathbb{C}}[\mathbf{F}_a^{-1} \otimes \mathbf{I}]. \tag{40}$$

The tangent moduli and the first Piola-Kirchhoff are then used to solve Equation (3).

4. Results

The algorithm described above has been implemented for the three-dimensional case. However, for illustration purpose, since the axonal growth on a substrate can be modeled as a two-dimensional problem, we will restrict ourselves to two-dimensional simulations here. All simulations were executed with the FEM module of *OXFEMM*, and spatial and temporal convergences were systematically tested. The parameters needed for the simulations as well as how they were obtained are presented in Appendix A.

4.1. Growth and retraction

This first study is aimed at exploring the axonal shaft growth and retraction in a constrained one-dimensional version of the two-dimensional ideal scenario, inspired by the current understanding about the interaction between growth cone and axonal shaft (O'Toole et al., 2015). Recently, Recho et al. (2016) proposed a one-dimensional theoretical model for neurite mechanical motility. This model recovers three different behaviors observed experimentally during neurite growth (Heidemann and Buxbaum, 1994). Depending on the normalized load $\hat{Q}$ at the interface between the axonal shaft and the growth cone, the axon would either grow (large $\hat{Q}$), stall (moderate $\hat{Q}$) or retract (low $\hat{Q}$). In this model two different domains in the axonal shaft are considered: the axoplasm and the cortical membrane. These regions are coupled through friction —unlike our computational model where the coupling is enforced by the shared nodes between the domains.

The load $\hat{Q}$ at the tip of the axonal shaft is defined by:

$$\hat{Q} = \underbrace{\frac{Q}{E_{micro}}}_{Q_{ext}} - \underbrace{\frac{k_p^{ap}}{k_d^{ap}\rho_0^{ap}}}_{Q_{ap}} \tag{41}$$

where the two terms Q_{ext} and Q_{ap} correspond to the external pressure applied to the axonal shaft scaled by the elasticity of the microtubules in the axoplasm, E_{micro}, and the pushing pressure of the axoplasm due to the microtubule dynamics, respectively (see Recho et al. (2016) for further information). The schematic representation of this scenario as well as the boundary conditions used are shown in Figure 5.

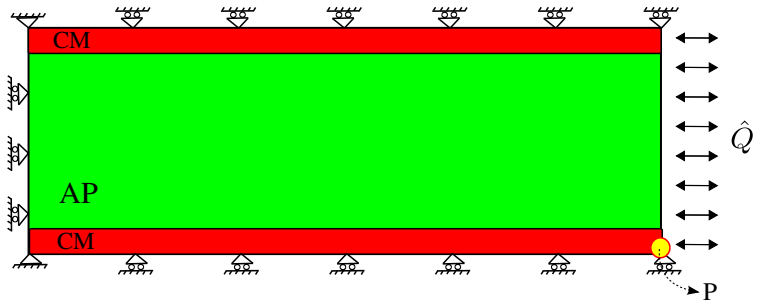

Figure 5: Growth and retraction in a constrained one-dimensional case. The point of study P is aimed at representing the movement of the tip of the axonal shaft at the interface with the growth cone.

In Figure 6, we show the results of the simulation as a function of $\hat{Q}$ and the ratio of viscosities $\varepsilon = \eta_{cm}/\eta_{ap}$, where η_{cm} and η_{ap} are the viscous coefficients of the cortical membrane and axoplasm, respectively.

Our computational model captures the threshold between the growth and collapse cases, see dashed lines in Figure 6. However, instead of having a static window between the motile and the collapse states (as in Recho et al. (2016)), the model exhibits a slow transition from collapse to growth as $\hat{Q}$ increases, see Figure 6-a. The model also exhibits a variation of v for small values of ε, see Figure 6-b. Interestingly, this variation in the growth rate for small ε has also a slight effect in the retraction case, see Figure 6-b.

4.2. Microtubule and F-actin dynamics participate to axonal turning

The cytoskeletal components are believed to play a major role in the determination of the axonal growth direction (Zhou and Cohan, 2003). More specifically, microtubule dynamics has been experimentally shown to participate to the directional steering of the axon (Buck and Zheng, 2002). Motivated by these studies, we explore how a local modification in microtubule dynamics, due to a mechanical constraint, leads the initiation of the turning response of the axon as dictated by the link between mechanics and cytoskeletal dynamics, i.e., Equations (13) and (18) for the axoplasm and cortical membrane.

The growth cone creates a force that pulls or pushes the axonal shaft at the interface by reading the extra-cellular biochemical and mechanical environment and interacting with the axonal shaft to create a

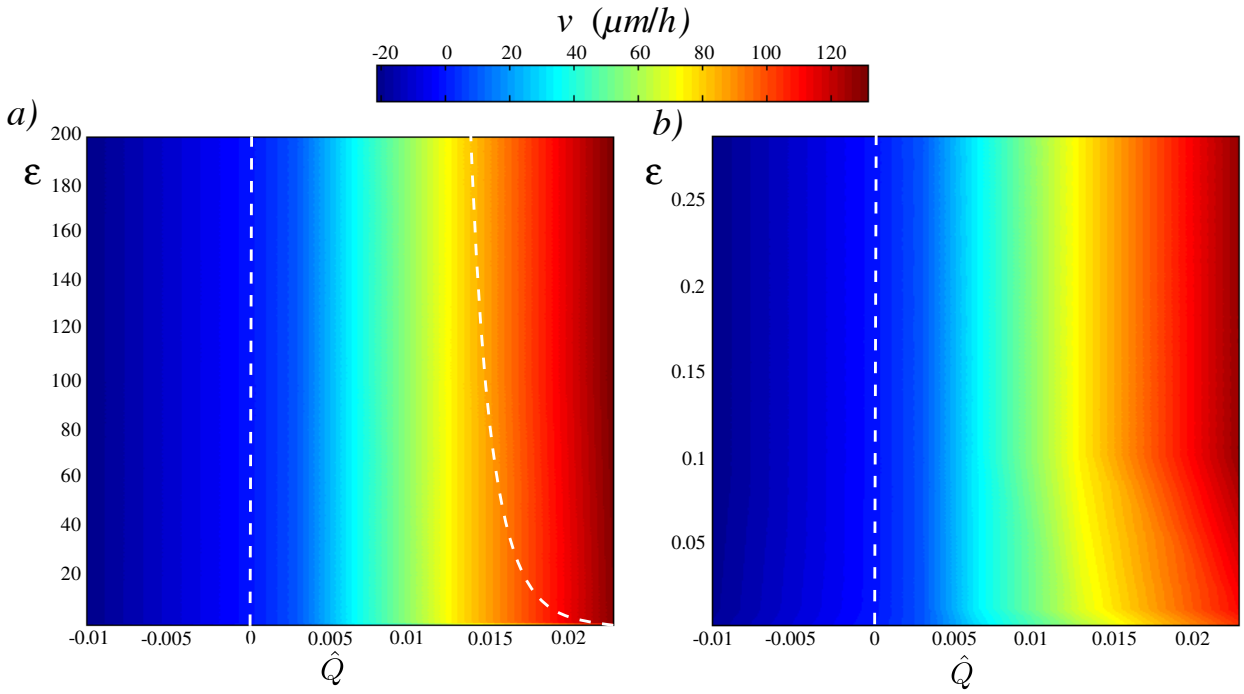

Figure 6: Growth and retraction in the one-dimensional setting schematically presented in Figure 5. The color map corresponds to the velocity of growth v at $t = 3000s$, taken as the time at which the growth reaches a constant rate, as a function of the viscosities of the axoplasm and cortical membrane, ε, and the normalized mechanical load $\hat{Q}$. For comparison, the theoretical predictions of Recho et al. (2016) are shown in dashed lines. The subfigure b) corresponds to a zoom-in for small values of ε. The corresponding movie is given in *GrowthCollapseAndStall.mp4*.

joint response. When turning upward, the growth cone creates a heterogeneous stress Q, that compresses the top half of the axonal shaft and stretches the bottom one, see inset in Figure 7. In this idealized scenario, the growth cone creates a force differential that pushes the axonal shaft turn upwards. We simulate this differential by using a Heaviside function. The external load applied in this example is $Q = 1Pa$. This load corresponds to $\hat{Q} = 6.13 \times 10^{-3}$, see Equation (41). This value promotes the axonal growth as shown in Figure 6. In order to further study the steering directional behavior of the axonal shaft, the load is applied during $600s$ and then removed. These conditions are designed to probe not only the turning when a load is applied, but also the behavior of the axonal shaft and the role of contractility after the load is removed. The local angle φ at the tip of the axonal shaft with respect to the horizontal line, see inset in Figure 7, is used as the measure of the turning ability of the axonal shaft.

Results are presented in Figure 7 for several c^0_{cm} and assuming that mechanics and growth are either coupled or uncoupled (enforced by taking $J = 1$ in Equations (13) and (18)). The axonal shaft turns after the instantaneous application of Q, due to the moment created. The load Q increases the growth rate at the bottom half of the axonal shaft (tension), while decreases it at the top half (compression), thus creating a transverse gradient of growth rate that increases the turning of (φ increases). In the uncoupled case, φ does not increase when holding Q, as expected from our discussion on polymerization predicting that the axonal shaft grows until it reaches an equilibrium. The evolution of φ is intertwined with the contractility rate c^0_{cm}. The larger is c^0_{cm}, the smaller φ is at the end of the application of Q. When the load is removed at $t = 600s$, φ instantaneously decreases, as expected by the elastic part of the deformation. Then, φ slowly decreases and the larger c^0_{cm} is the faster the axonal shaft goes back to its initial direction before applying Q. When there is no growth, the turning behavior was similar to the uncoupled case (not shown here).

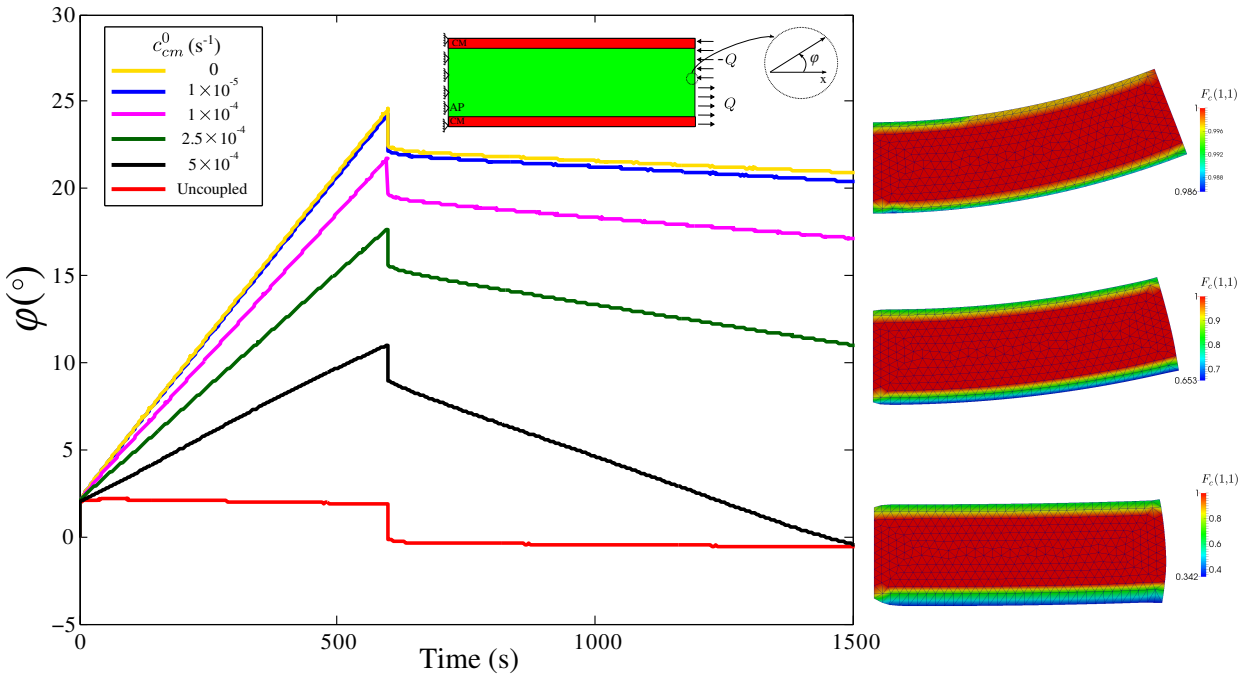

Figure 7: Axonal guidance by axonal shaft steering due to cytoskeletal dynamics. Top *inset*: schematic representation of the idealized scenario. A heterogeneous external load Q is imposed by the growth cone during $600s$. Some deformed shapes at $t = 1500s$ are also presented on the right hand side with the color map corresponding to contractility. *Main plot*: evolution of φ during the time for different cases: without contraction, several contractility rates and uncoupling the cytoskeletal dynamics and the mechanics. The corresponding movie is given in *Supplementary Material: AxonalTurning.mp4*.

5. Discussion

A computational continuum framework for modeling axonal outgrowth has been developed. The model focuses particularly on axonal shaft development by identifying two different regions: the axoplasm, where its dynamics is governed by the microtubules, and the cortical membrane, that surrounds the axoplasm and includes the F-actin, Myosin motor proteins and the membrane. The model relies on the decomposition of the deformation gradient into anelastic and viscoelastic parts. For the former contribution, the final mathematical representation is a growth tensor with an extra contribution from contractility for the cortical membrane, while for the latter, a viscoelastic constitutive model is used. Notably, based on the equilibrium equations, the coupling between growth and mechanics is naturally obtained (as observed experimentally Dennerll et al. (1989); Zheng et al. (1991)). We use our framework to model two different scenarios: growth and retraction, and axonal turning.

The growth and retraction study is used to validate our framework against the theoretical work done by Recho et al. (2016). The three scenarios discussed in the literature, i.e., growth, stall, and collapse (Heidemann and Buxbaum, 1994), were not directly recovered in our model. Our model being completely dynamic, it is unlikely that a true stall state would be recovered without using large friction between the axonal shaft and the extra-cellular matrix in the model. However, our model does capture correctly the transition between the collapse and growth states. The model also confirms that larger loads $\hat{Q}$ lead to larger velocities v. More interesting, for small ε, larger $\hat{Q}$ is needed to accelerate the growth of the axonal shaft. This trend is in agreement with the jump between the static and motile states observed in Recho et al. (2016).

At the theoretical and computational level, axonal guidance is still a largely unexplored problem. The complex interaction between the extra-cellular matrix, the growth cone and the axonal shaft, leads to an orchestrated phenomenon in which the isolation of each potential contributor is technically difficult or impossible to observe experimentally (Franze and Guck, 2010; Goodhill, 2016). Computational studies may

be particularly helpful to establish the roles of each effects separately or coupled. Here, a natural link between the cytoskeletal dynamics and the mechanical response was proposed (see Equations (13) and (18) for the axoplasm and cortical membrane, respectively). Although a form for the growth rate has been already proposed for axonal steering modulator under constrained substrates (Mortimer et al., 2010), our model explicitly confirms that even a small gradient imposed by the growth cone can trigger a series of growth and contraction phenomena able to turn the whole axonal shaft. Indeed, this gradient modifies locally the rates of growth, creating a moment that contributes to axonal shaft steering and thus axonal guidance. Practically, the mechanical load Q needed to make the axon turn by $\varphi \sim 24°$ (see Figure 7) in the uncoupled case would be ~ 10 times larger than the one needed with the cytoskeletal contributions. Our study therefore suggests that the growth cone load Q may act as an important growth rate modulator that triggers the heterogeneous cytoskeletal activity in the axonal shaft, eventually fuelling axonal turning.

Cortical membrane contractility was shown to play a key role in this scenario for axonal steering. It depends on the local tension state, see Equation (20), and acts in the bottom region opposing the turning. Therefore, the larger c^0_{cm} the smaller the final angle is. Furthermore, as this contractility does not disappear after removing the load, the higher the contractility, the faster the axonal shaft goes back to its initial direction. Without contraction, the angle decreases slowly. Contractility thus appears as a possible mechanism to correct the axonal shaft final direction after a mechanical external load. An important addition to the model proposed here is to consider the interaction with the surrounding substrate, which could lead to a sustained steering effect, even after removal of the loading force Q.

Acknowledgements

A.J. acknowledges funding from the European Union's Seventh Framework Programme (FP7 20072013) ERC Grant Agreement No. 306587. The authors would like to thank Dr Pierre Recho and Prof. Ellen Kuhl for very productive discussions.

Appendix A. Parameters space

Geometry. The axonal shaft is considered as a $10\mu m$ diameter cylinder, with a length of $30\mu m$. Both values are aimed at encompassing a typical axon after neurite differentiation (Goslin and Banker, 1989; Esch et al., 1999; Lewis et al., 2013). The thickness of cortical membrane is $0.5\mu m$ (Xu et al., 2013), leading to an axoplasm of $9\mu m$ in diameter.

Stored-energy function. The chosen hyperelastic stored-energy function (see Equation (24)) is defined by:

$$W^o(\mathbf{C}) = \underbrace{\frac{1}{2}\kappa\left((J^2-1)-\ln J\right)}_{U^o(J)} + \underbrace{\frac{1}{2}\mu\left(\mathrm{tr}[\bar{\mathbf{C}}]-3\right)}_{\bar{W}^o(\bar{\mathbf{C}})} \tag{A.1}$$

where $U^o(J)$ and $\bar{W}^o(\bar{\mathbf{C}})$ correspond to the volumetric and volume-preserving energetic contributions, respectively. The mechanical properties of the material are defined by κ, the bulk modulus, and μ, the shear modulus (Simo and Hughes, 1998). Note that the material is assumed isotropic with a neo-Hookean elastic part. Because of the microtubules alignment, we expect that as a three-dimensional material, the response of the axoplasm would nevertheless be anisotropic. However, the correct modeling of the anisotropic response of axons is an open problem and, in the first instance, we isolate the effect of anisotropic growth fromanisotropic mechanics by assuming an isotropic mechanical response.

Axoplasm parameters. The parameters that should be defined are: κ_{ap}, $\mu^{ap}_\infty + \mu^{ap}$, k^{ap}_p, k^{ap}_d and ρ^{ap}_0. While κ_{ap}, $\mu^{ap}_\infty + \mu^{ap}$ are purely mechanical, k^{ap}_p, k^{ap}_d and ρ^{ap}_0 are the kinematic parameters that govern the growth of the axoplasm, and as such, the net velocity of growth. ρ^{ap}_0 is the density of microtubules in a given volume of axonal shaft in kg/m^3, while the units of k^{ap}_p and k^{ap}_d are $kg/m^3 s$ and s^{-1}, respectively. The number of microtubules per cross sectional area of the axon is 10—200 μm^{-2} (Peter and Mofrad,

2012). Considering a constant concentration of tubulin dimers of $\sim 5\mu M$ (see Recho et al. (2016) for a discussion on the approximation of constant concentration), a microtubule polymerizes and depolymerizes at $\sim 1.65\mu m/min$ and $\sim 1.59\mu m/min$, respectively (Walker et al., 1988). Taking into account that to cover $1\mu m$ of microtubule, $\sim 1,625$ dimers are needed (Conde and Cáceres, 2009; Hawkins et al., 2010), the polymerization/depolymerization rates thus become $2,681.25$ $dimers/min$ and $2,583.75$ $dimers/min$ for each microtubule. We thus estimate the following values: $k_p^{ap} = 0.0295$ $kg/m^3 s$, $k_d^{ap} = 0.0265$ s^{-1} and $\rho_0^{ap} = 1.1101$ kg/m^3, based on: the initial volume of the axoplasm at its initial state, the number of microtubules in a particular cross sectional area ($10\mu m$ in diameter of the axon, see Walker et al. (1988)), and the mass of a tubulin dimer $1.660539 \times 10^{-22} kg/dimer$ (Biswas and Roy, 1995). These kinematic values finally lead to velocity of growth around $\sim 10\mu m/h$. The remaining mechanical properties are taken from the literature and are shown in Table A.1.

Cortical membrane parameters. The parameters needed for the cortical membrane are the same as for the axoplasm, i.e., K_{cm}, $\mu_\infty^{cm}+\mu^{cm}$, k_p^{cm}, k_d^{cm} and ρ_0^{cm}, plus two additional parameters related to the contractility in the cortical membrane, i.e., c_0^{cm} and σ_0. The first assumption is that the cortical membrane follows the evolution of the axoplasm during the microtubule dynamics inside the axoplasm. This is motivated by the fact that the F-actin dynamics is faster than the microtubules dynamics (Coles and Bradke, 2015; Betz et al., 2011), and thus the cortical membrane will follow the growth/retraction of the axoplasm when required (Recho et al., 2016). That assumption implies that $k_p^{cm} = k_p^{ap}$, $k_d^{cm} = k_d^{ap}$ and $\rho_0^{cm} = \rho_0^{ap}$. Finally, the mechanical properties of the cortical membrane are taken from the literature, while the contractility related values were studied in Section 7 and estimated from the literature. See Table A.1.

Table A.1: Parameters of the simulations

Parameter	Symbol	Value	Units	Reference
Axon Diameter	d_0	10	μm	-
Initial length of the axon	L_0	30	μm	Goslin and Banker (1989); Esch et al. (1999); Lewis et al. (2013)
Microtubules per cross sectional area	-	~ 105	$\mu^{-1}m^{-2}$	Peter and Mofrad (2012)
Concentration of tubulin dimers	-	~ 5	μM	Walker et al. (1988)
AP polymerization rate constant	k_p^{ap}	0.0295	$kg/m^3 s$	see *AP parameters* paragraph
AP depolymerization rate constant	k_d^{ap}	0.0265	s^{-1}	see *AP parameters* paragraph
AP density	ρ_0^{ap}	1.1101	kg/m^3	see *AP parameters* paragraph
AP bulk Modulus	κ^{ap}	~ 250	Pa	Recho et al. (2016)
AP shear modulus	μ_∞^{ap}	~ 57.5	Pa	Recho et al. (2016)
AP shear modulus	μ^{ap}	~ 57.5	Pa	Recho et al. (2016)
AP viscosity	η^{ap}	1×10^6	$Pa.s$	O'Toole et al. (2008, 2015)
CM thickness	-	0.5	μm	Jülicher et al. (2007)
CM polymerization rate constant	k_p^{cm}	0.0295	$kg/m^3 s$	*CM parameters* paragraph
CM depolymerization rate constant	k_d^{cm}	0.0265	s^{-1}	*CM parameters* paragraph
CM density	ρ_0^{cm}	1.1101	kg/m^3	*CM parameters* paragraph
AP bulk Modulus	κ^{cm}	~ 158	Pa	Recho et al. (2016)
AP shear modulus	μ_∞^{cm}	~ 73	Pa	Recho et al. (2016)
AP shear modulus	μ^{cm}	~ 73	Pa	Recho et al. (2016)
CM viscosity	η^{ap}	1×10^3	$Pa.s$	Betz et al. (2011)
Initial contractility	c_0	1×10^{-5}	s^{-1}	Estimated
Stress threshold	σ_0	30	Pa	Estimated

References

Aeschlimann, M., 2000. Biophysical models of axonal pathfinding. Ph.D. thesis, Université de Lausanne.

Aeschlimann, M., Tettoni, L., 2001. Biophysical model of axonal pathfinding. Neurocomputing 38–40, 87–92.

Ahmadzadeh, H., Smith, D., Shenoy, V., 2014. Viscoelasticity of Tau protein leads to strain rate-dependent breaking of microtubules during axonal stretch injury: predictions from a mathematical model. Biophysical Journal 106, 1123–1133.

Ambrosi, D., Ateshian, G., Arruda, E., Cowin, S., Dumais, J., Goriely, A., Holzapfel, G., Humphrey, J., Kemkemer, R., Kuhl, E., Olberding, J., Taber, L., Garikipati, K., 2011. Perspectives on biological growth and remodeling. Journal of the Mechanics and Physics of Solids 59, 863–883.

Athamneh, A., Suter, D., 2015. Quantifying mechanical force in axonal growth and guidance. Frontiers in Cellular Neuroscience 9, 1–8.

Baas, P., Deitch, J., Black, M., Banker, G., 1988. Polarity orientation of microtubules in hippocampal neurons: Uniformity in the axon and nonuniformity in the dendrite. PNAS 85, 8335–8339.

Ben Amar, M., Goriely, A., 2005. Growth and instability in elastic tissues. J. Mech. Phys. Solids 53 (10), 2284–2319.

Bernal, R., Pullarkat, P., Melo, F., 2007. Mechanical properties of axon. Physical Review letters 99, 018301.

Betz, T., Koch, D., Lu, Y.-B., Franze, K., K as, J., 2011. Growth cones as soft and weak force generators. PNAS 106, 13420–13425.

Biswas, B., Roy, S., 1995. Subcellular biochemistry. Proteins: structure, function and engineering. Springer Science + Business Media, LLC.

Bradke, F., Fawcett, J., Spira, M., 2012. Assembly of a new growth cone after axotomy: the precursor to axon regeneration. Nature Reviews Neuroscience 13, 183–193.

Buck, K., Zheng, J., 2002. Growth cone turning induced by direct local modification of microtubule dynamics. The Journal of Neuroscience 22, 9358–9367.

Budday, S., Raybaud, C., Kuhl, E., 2014. A mechanical model predicts morphological abnormalities in the developing human brain. Scientific Reports 4, 5644.

Budday, S., Steinmann, P., Goriely, A., Kuhl, E., 2015. Size and curvature regulate pattern selection in the mammalian brain. Extreme Mechanics Letters 4, 193–198.

Cajal, S. R., 1909. Histologie du système nerveux de l'homme & des vertébrés. Paris, A. Maloine.

Case, L., Tessier-Lavigne, M., 2005. Regeneration of the adult central nervous system. Current Biology 15, R749–R753.

Coles, C., Bradke, F., 2015. Coordinating neuronal actin-microtubule dynamics. Current Biology 25, R677–R691.

Conde, C., Cáceres, A., 2009. Microtubule assembly, organization and dynamics in axons and dendrites. Nature Reviews. Neuroscience 10, 319–332.

Curnier, A., 1994. Computational methods in solid mechanics. Springer.

Debanne, D., Campanac, E., Bialowas, A., Carlier, E., Alcaraz, G., 2011. Axon physiology. Physiological Revies 91, 555–602.

DeFelipe, J., Jones, E., 1988. Cajal on the cerebral cortex: an annotated translation of the complete writings. New York: Oxford University Press.

Dennerll, T., Lamoureux, P., Buxbaum, R., Heidemann, S., 1989. The cytomechanics of axonal elongation and retraction. The Journal of Cell Biology 109, 3073–3083.

Dent, E., Gupton, S., Gertler, F., 2011. The growth cone cytoskeleton in axon outgrowth and guidance. Cold Spring Harb Perspect Biol 3, a001800.

Diehl, S., Henningsson, E., Heyden, A., 2016. Efficient simulation of tubuli-driven axonal growth. Journal of Computational Neuroscience, 1–19.

Diehl, S., Henningsson, E., Heyden, A., Perna, S., 2014. A one-dimensional moving-boundary model for tubulin-driven axonal growth. Journal of Theoretical Biology 358, 194–207.

Dogterom, M., Kerssemakers, J., Romet-Lemonne, G., Janson, M., 2005. Force generation by dynamic microtubules. Current Opinion in Cell Biology 17, 67–74.

Dogterom, M., Yurke, B., 1997. Measurement of the force-velocity relation for growing microtubules. Science 279, 856–860.

Edward, K., 2009. Cell biology of the axon. Springer.

Esch, T., Lemmon, V., Banker, G., 1999. Local presentation of substrate molecules directs axon specification by cultured hippocampal neurons. J. Neurosci. 19, 6417–6426.

Eskandari, M., Kuhl, E., 2015. Systems biology and mechanics of growth. WIREs Syst Biol Med 7, 401–412.

Fletcher, D., Mullins, R., 2010. Cell mechanics and the cytoskeleton. Nature rev 468, 485–492.

Foisner, R., 2002. Intermediate filaments. Encyclopedia of Lige Sciences, 1–9.

Franze, K., Guck, J., 2010. The biophysics of neuronal growth. Reports on Progresss in Physics 73, 094601.

García, J., na, J. P., McHugh, S., Jérusalem, A., 2012. A model of the spatially dependent mechanical properties of the axon during its growth. CMES 87, 411–432.

Geraldo, S., Gordon-Weeks, P., 2009. Cytoskeletal dynamics in growth-cone steering. Journal of Cell Science 122, a001800.

Goldberg, J., 2003. How does an axon grow. Genes & Development 17, 941–958.

Gomez, T., Letourneau, P., 2014. Actin dynamics in growth cone motility and navigation. Journal of Neurochemistry 129, 221–234.

Goodhill, G., 2016. Can molecular gradients wire the brain? Trends in Neurosciences in press.

Goodhill, G., Faville, R., Sutherland, D., Bicknell, B., Thompson, A., Pujic, Z., Sun, B., Kita, E., Scott, E., 2015. The dynamics of growth cone morphology. BMC Biology 13, 1–18.

Goriely, A., Budday, S., Kuhl, E., 2015a. Chapter two— Neuromechanics: from neurons to brain. Advances in Applied Mechanics 48, 79–139.

Goriely, A., Geers, M., Holzapfel, G., Jayamohan, J., Jérusalem, A., Sivaloganathan, S., Squier, W., van Dommelen, J., Waters, S., Kuhl, E., 2015b. Mechanics of the brain: perspectives, challenges, and opportunities. Biomechanis and Modelling in Mechanobiology 14, 931–965.
Goriely, A., Moulton, D. E., 2010. Morphoelasticity - a theory of elastic growth. In: Press, O. U. (Ed.), New Trends in the Physics and Mechanics of Biological Systems.
Goriely, A., Moulton, D. E., Vandiver, R., 2010. Elastic cavitation, tube hollowing, and differential growth in plants and biological tissues. EPL (Europhysics Letters) 91 (1), 18001.
Goslin, K., Banker, G., 1989. Experimental observations on the development of polarity by hippocampal neurons in culture. J. Cell. Biol. 108, 1507–1516.
Graham, B., Lauchlan, K., Mclean, D., 2006. Dynamics of outgrowth in a continnuum model of neurite elongation. J. Comput. Neurosci. 20, 43–60.
Graham, B., van Ooyen, A., 2001. Compartmental models of growing neurites. Neurocomputing 38-40, 31–36.
Grevesse, T., Dabiri, B., Parker, K., Gabriele, S., 2015. Opposite rheological properties of neuronal microcompartments predict axonal vulnerability in a brain injury. Scientific Reports 5, 1–10.
Hawkins, T., Mirigian, M., Yasar, M., Ross, H., 2010. Mechanics of microtubules. Journal of Biomechanics 43, 23–30.
Heidemann, S., Buxbaum, R., 1994. Mechanical tension as a regulator of axonal development. NeuroToxicology 15, 95–108.
Himpel, G., Kuhl, E., Menzel, A., Steinmann, P., 2005. Computational modelling of isotropic multiplicative growth. Computer Modeling in Engineering & Sciences 8, 119–134.
Holland, M., Miller, K., Kuhl, E., 2015. Emergin brain morphologies from axonal elongation. Annals of Biomedical Engineering 43, 1640–1653.
Javid, S., Rezaei, A., Karami, G., 2014. A micromechanical procedure for viscoelastic charaterization of the axons and ECM of the brainstem. Journal of the Mechanical Behavior of Biomedical Materials 30, 290–299.
Jülicher, F., Kruse, K., Prost, J., Joanny, J.-F., 2007. Active behaviour of the cytoskeleton. Physics Reports 449, 3–28.
Kuhl, E., 2014. Growing matter: a review of growth in living systems. Journal of the Mechanical Behavior of Biomedical Materials 29, 529–543.
Lafont, F., Rouget, M., Rousselet, A., Valenza, C., Prochiantz, A., 1993. Specific responses of axons and dendrites to cytoskeleton perturbations: an *in vitro* study. Journal of Cell Science 104, 433–443.
Lamoureux, P., Buxbaum, R., Heidemann, S., 1989. Direct evidence that growth cones pull. Nature 340, 159–162.
Lamoureux, P., Buxbaum, R., Heidemann, S., 1998. Axonal outgrowth of cultured neurons is not limited by growth cone competition. Journal of Cell Science 111, 3245–3252.
Lewis, T., Courchet, J., Polleux, F., 2013. Cellular and molecular mechanisms underlying axon formation, growth and branching. the Journal of Cell Biology 202, 837–848.
Lu, Y.-B., Franze, K., Seifert, G., Steinh auser, C., Kirchhoff, F., Wolburg, H., Guck, J., Janmey, P., Wei, E.-Q., K as, J., Reichenbach, A., 2006. Viscoelastic properties of individual glial cells and neurons in the CNS. PNAS 103, 17759–11764.
Marsh, L., Letourneau, P., 1984. Growth of neurites without filopodial or lamellipodial activity in the presence of cytochalasin B. Journal of Cell Biology 99, 2041–2047.
McLean, D., van Ooyen, A., Graham, B., 2004. Continuum model for tubulin-driven neurite elongation. Neurocomputing 58-60, 511–516.
Miller, M., Samuels, D., 1997. The axon as a metabolic compartment: protein degradation, transport and maximum length of an axon. J. theor. Biol. 186, 373–379.
Mitchinson, T., Kirschner, M., 1988. Cytoskeletal dynamics and nerve growth. Neuron 1, 761–772.
Mortimer, D., Pujic, Z., Vaughan, T., Thompson, A., Feldner, J., Vetter, I., Goohill, G., 2010. Axon guidance by growth-rate modulation. PNAS 107, 5202–5207.
Moulton, D. E., Goriely, A., 2011. Possible role of differential growth in airway wall remodeling in asthma. J. Applied Physiol. 110 (4), 1003–1012.
O'Toole, M., Lamoureux, P., Miller, K., 2008. A physical model of axonal elongation: force, viscosity, and adhesions govern the mode of outgrowth. Biophysical Journal 94, 2610–2620.
O'Toole, M., Lamoureux, P., Miller, K., 2015. Measurement of subcellular force generation in neurons. Biophysical Journal 108, 1027–1037.
Pascual-Leone, A., Amedi, A., Fregni, F., Merabet, L., 2005. The plastic human brain cortex. Annual Review of Neuroscience 28, 377–401.
Pasik, P., Pasik, T., 1999. Texture of the nervous system of man and the vertebrates. Springer.
Peter, S., Mofrad, M., 2012. Computational modeling of axonal microtubule bundles under tension. Biophys. J. 102, 749–757.
Poulain, F., Sobel, A., 2010. The microtubule network and neuronal morphogenesis: Dynamics and coordinated orchestration through multiple players. Molecular and Cellular Neuroscience 43, 15–32.
Recho, P., Jérusalem, A., Goriely, A., 2016. Growth, collapse, and stalling in a mechanical model for neurite motility. Physical Review E 12, under review.
Roccasalvo, I., Micera, S., Sergi, P., 2015. A hybrid computational model to predict chemotactic guidance of growth cones. Scientific Reports 5, 11340.
Rodriguez, E., Hoger, A., McCulloch, A., 1994. Stress dependent finite growth in soft elastic tissues. Annals of Biomedical Engineering 43, 1640–1653.
Silver, J., Miller, J., 2004. Regeneration beyond the glial scar. Nature Reviews Neuroscience 5, 146–156.
Simo, J., Hughes, T., 1998. Computational inelasticity. Springer.
Stiess, M., Bradke, F., 2009. Cytoskeleton in axon growth. Encyclopedia of Lige Sciences, 1–9.
van Ooyen, A., 2011. Using theoretical models to analyse neural developement. Nature Reviews Neuroscience 12, 311–326.

van Ooyen, A., Graham, B., Ramakers, G., 2001. Competition for tubulin between growing neurites during development. Neurocomputing 38, 73–78.
van Veen, M., van Pelt, J., 1994. Neuritic growth rate described by modeling microtubule dynamics. Bull Math Biol 56, 249–273.
Walker, R., O'Brien, E., Pryer, N., Soboeiro, M., Voter, W., Ericks, H., Salmon, E., 1988. Dynamic instability of individual microtubules analyzed by video light microscopy: rate constants and transition frequencies. Journal of Cell Biology 107, 1437–1448.
Xu, K., Zhong, G., Zhuang, X., 2013. Actin, spectring, and associated proteins form a periodic cytoskeletal structure in axons. Science 339, 452–456.
Zheng, J., Lamoureux, P., Santiago, V., Dennerll, T., Buxbaum, R., Heidemann, S., 1991. Tensile regulation of axonal elongation and initiation. The Journal of Neuroscience 11, 1117–1125.
Zhou, F., Cohan, C., 2003. How actin filaments and microtubules steer growth cones to their targets. Journal of Neurobiology 58, 84–91.
Zubler, F., Douglas, R., 2009. A framework for modeling the growth and development of neurons and networks. Frontiers in Computational Neuroscience 3, 25.
Prevost, T.P., Balakrishnan, A., Suresh, S., Socrate, S. Biomechanics of brain tissue. Acta Biomaterialia 7, 83-95.
de Rooij, R., Kuhl, E. Constitutive Modeling of Brain Tissue: Current Perspectives. Applied Mechanics Reviews 68, 010801.